*metals*

MDPI

*Article*

# A Physically Based Model Predicting the Degradation of Hydrogen on Crack Growth Critical Stress Intensity Factor of Metals

**Yuting Huang [1], Jihan Chen [1], Yanfei Wang [1,*], Wei Liu [1], Weijie Wu [2,*], Xinfeng Li [3] and Xinyu Yang [4]**

[1] School of Chemical Engineering and Technology, China University of Mining and Technology, Xuzhou 221116, China
[2] Institute for Advanced Materials and Technology, University of Science and Technology Beijing, Beijing 100083, China
[3] Sino-French Institute of Nuclear Engineering and Technology, Sun Yat-sen University, Zhuhai 519082, China
[4] Mechanical Engineering, School of Engineering, College of Science and Engineering, National University of Ireland, H91 HX31 Galway, Ireland
* Correspondence: wyf_hg@cumt.edu.cn (Y.W.); wjwu163@163.com (W.W.)

**Abstract:** A simple, physically based model is developed to quantitatively predict the degradation of hydrogen on the crack growth critical stress intensity factor (CSIF) of metals. The model is formulated by combining a microscopically shielded Griffith criterion (MSGC) model for plasticity-induced cleavage fracture and thermodynamics decohesion (TDD) theory for hydrogen-enhanced interface decohesion. The hydrogen-influenced CSIF is described as a function of the intrinsic CSIF (hydrogen-free), initial hydrogen concentration (solubility), hydrogen trap binding energy and crack tip stress. All parameters in the model can be determined with a physical basis and the model is successfully validated by comparison with published experimental data.

**Keywords:** hydrogen-assisted fracture; hydrogen embrittlement; critical stress intensity factor; hydrogen-enhanced decohesion

check for updates

**Citation:** Huang, Y.; Chen, J.; Wang, Y.; Liu, W.; Wu, W.; Li, X.; Yang, X. A Physically Based Model Predicting the Degradation of Hydrogen on Crack Growth Critical Stress Intensity Factor of Metals. *Metals* **2022**, *12*, 1441. https://doi.org/10.3390/met12091441

Academic Editors: Francesco Iacoviello and Leu-Wen Tsay

Received: 7 May 2022
Accepted: 22 August 2022
Published: 29 August 2022

**Publisher's Note:** MDPI stays neutral with regard to jurisdictional claims in published maps and institutional affiliations.

**Copyright:** © 2022 by the authors. Licensee MDPI, Basel, Switzerland. This article is an open access article distributed under the terms and conditions of the Creative Commons Attribution (CC BY) license (https://creativecommons.org/licenses/by/4.0/).

## 1. Introduction

Crack growth criteria in fracture mechanics have been widely used for the design and safety assessment of metallic components. Particularly, the $K$ criterion, which defines a crack under mode I loading in a component will not grow if $K_I \leq K_{IC}$, where $K_I$ is the stress intensity factor (SIF) of the crack and $K_{IC}$ is the critical stress intensity factor (CSIF, also known as fracture toughness) of material used for the component. However, the components serving in hydrogen-containing environments often suffer from hydrogen-assisted fracture (HAF) under lower stresses ($K_I \leq K_{IC}$), leading to "brittle" failures. It is necessary to develop a physically based model to accurately predict the degradation of hydrogen on fracture critical parameters, i.e., the CSIF with hydrogen influence ($K_{IH}$).

Many models [1–13] have already been reported with the development of HAF mechanism such as hydrogen-enhanced decohesion (HEDE) [1–4] and hydrogen-enhanced localized plasticity (HELP) [3,14,15]. However, these models often involve empirical parameters to take account of the effect from physical mechanisms. For example, by assuming that the local fracture stress (energy) decreases linearly with the increase of local hydrogen concentration, Gerberich et al. [1–3], Oriani and Josephic [6,7], Akhurst and Baker [8], Lee and Unger [9], Unger [10] and Wang et al. [12] proposed models to describe the hydrogen-influenced macroscopic crack growth critical values, including the CSIF. Corresponding coefficients describing the negative correlation between local fracture stress and hydrogen concentration are empirical, unknown in advance due to the physical origins being unclear. In fact, they can only be determined by fitting the experimental data with developed mathematical description. Although these models can fit experimental data with small deviations [1–3,6–10,12] and have been widely used [16–22], the unpredictability of these

empirical parameters limit the effectiveness and applicability of these models and the physical origins of the empirical parameters need to be clarified [23,24].

The thermodynamics decohesion (TDD) theory of interface separations induced by adsorbed solute atmospheres was established by Hirth and Rice [25] and Wang [26]. It provides criterion for interfacial decohesion from the view of thermodynamics of adsorption. In recent years, the TDD-based criterion has been implemented in coupled mechanical-diffusion finite element analysis to calculate stresses, strains and hydrogen concentration field around a crack tip or an inclusion or in molecular dynamics simulations of crack tip and has been found capable of reproducing the experimental trends [27–30].

In addition, Gerberich et al. [1–3,31–33] have developed a microscopically-shielded Griffith criterion (MSGC) model to predict the macroscopic crack growth CSIF for cleavage fracture of semibrittle materials. The model was found capable of predicting the CSIF of many materials such as the Fe-Si polycrystalline material [31–33].

In this paper, we combine the MSGC model and TDD theory to form a physically based model to study the crack along cleavage planes or grain boundaries in the context of HAF. In this model, all parameters are physically based and can be measured or calculated in advance. More importantly, the model is simple and convenient to provide accurate predictions which are validated by comparing with published experimental data.

## 2. Methodology

In order to evaluate the role of crack tip emission and shielding of near-tip dislocations in cleavage fracture of semibrittle materials, Gerberich et al. [31–33] developed a discretized dislocation model consisting of five single dislocations near the tip and a giant super-dislocation for far field. Based on two-dimensional computational simulations using the microscopic Griffith fracture criterion, the MSGC-based model is developed as [31–33]:

$$K_{IC} = \frac{1}{\beta'} \exp\left[\frac{{k_{IG}}^2}{\alpha'' \sigma_{ys}}\right] \tag{1}$$

where $K_{IC}$ is the CSIF under mode I loading, $k_{IG}$ is the local microscopic Griffith stress intensity for fracture in plane strain, $\sigma_{ys}$ is yield strength and $\alpha''$ and $\beta'$ are crack tip stress field constants, which can be determined from the computational simulations. Thus, the interplay between crack tip plasticity and stress-based decohesion is captured by the MSGC model to give accurate an prediction of $K_{IC}$ [1–3,31–33]. In order to extend the model to include hydrogen influence, Gerberich et al. [1–3] assumed that the local Griffith stress intensity decreases linearly with the increment of local hydrogen concentration, as:

$$K_{IH} = \frac{1}{\beta'} \exp\left[\frac{(k_{IG} - \alpha C_H)^2}{\alpha'' \sigma_{ys}}\right] \tag{2}$$

where $K_{IH}$ is the CSIF with hydrogen influence, $C_H$ is the hydrogen concentration at the potential cracking site ahead of the crack tip, and $\alpha$ is a constant representing the decreasing rate of $k_{IG}$ with the increment of hydrogen concentration. That is, hydrogen-influenced local microscopic Griffith stress intensity $k_{IGH}$ is assumed as $k_{IGH} = k_{IG} - \alpha C_H$. It is worth nothing that $\alpha$ is not physically determined and is often obtained by fitting against experimental data for a given material [1,2,6–10,12,16–22].

According to the microscopic Griffith fracture criterion, for the separation of an interface, the $k_{lG}$ can be expressed as a function of the effective work of decohesion $\gamma_{eff}$ of the interface, which is the sum of the reversible work of decohesion $2\gamma^0_{int}$ and plastic work $\gamma_P$. If plastic work is not considered for semibrittle materials, $\gamma_{eff}$ equals to $2\gamma^0_{int}$, therefore [32]

$$k_{IG} = \sqrt{\frac{2\gamma^0_{int} E}{1 - \nu^2}} \tag{3}$$

where $E$ is Young's modulus, $\nu$ is Poisson rate and $2\gamma_{int}^{0}$ is the reversible work of decohesion in absence of hydrogen. According to the Langmuir–McLean adsorption isotherm, Novak et al. [28] and Jung et al. [29] proposed a physically based expression for the TDD theory built by Hirth and Rice [25] and Wang [26], describing the degradation of cohesive energy when hydrogen is introduced:

$$2\gamma_{int}^{H} = 2\gamma_{int}^{0} - \left(\Delta g_{int}^{0} - \Delta g_{FS}^{0}\right)\Gamma \tag{4}$$

where $2\gamma_{int}^{H}$ is hydrogen-influenced cohesive energy, $\Delta g_{int}^{0}$ and $\Delta g_{FS}^{0}$ ($\Delta g^{0} = \Delta h^{0} - T\Delta S^{0}$, $\Delta h^{0}$ is enthalpy change, $\Delta S^{0}$ is entropy change, and $T$ is temperature) are Gibbs free energy excesses when hydrogen is segregated to the interface and absorbed onto the free surfaces (FS) created by separation of the interface, respectively, and $\Gamma$ is hydrogen coverage of the interface defined as the number of atoms per unit area of interface. With the consideration of a monolayer hydrogen coverage, the hydrogen coverage $\Gamma$ can be related to hydrogen occupancy $\theta_H$ of the interface (taken as hydrogen traps) by $\Gamma/\Gamma_{max} = \theta_H$ [25–29], where $\Gamma_{max}$ is the saturated hydrogen coverage. Therefore, Equation (4) can be rewritten as

$$\frac{2\gamma_{int}^{H}}{2\gamma_{int}^{0}} = 1 - \eta\theta_H \tag{5}$$

where

$$\eta = \frac{\left(\Delta g_{int}^{0} - \Delta g_{FS}^{0}\right)\Gamma_{max}}{2\gamma_{int}^{0}} \tag{6}$$

Equation (5) can be verified by first-principle calculations (density functional theory methods). As shown in Figure 1, Jiang and Carter [34] obtained the cohesive energy of Fe(110) and Al(111) crystal interface using first-principle calculations, and Jensen et al. [35] calculated the cohesive energy of Ni-∑5(012) grain boundary. It is shown that when $\theta_H < 1$ (monolayer coverage), cohesive energy is reduced approximately linearly by increase of $\theta_H$. The linear coefficient $\eta$ obtained by fitting the data using Equation (4) is shown in Figure 1.

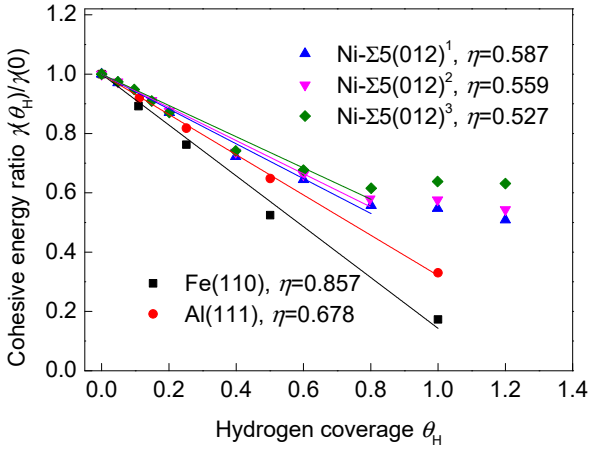



**Figure 1.** Effect of hydrogen coverage on cohesive energy of Fe(110), Al(111) crystal interface [34] and Ni-∑5(012) grain boundary [35] (Ni-∑5(012) grain boundary has three sets of data due to different calculation schemes used by the authors).

According to Equation (3), the hydrogen-influenced local microscopic Griffith stress intensity $k_{IGH}$ can be expressed as $k_{IGH} = k_{IG}\sqrt{(1 - \eta\theta_H)}$. Therefore, the hydrogen-influenced CSIF $K_{IH}$ can be formulated as:

$$K_{IH} = \frac{1}{\beta'}\exp\left[\frac{{k_{IG}}^2(1 - \eta\theta_H)}{\alpha''\sigma_{ys}}\right] \tag{7}$$

Incorporating Equation (1), $K_{IH}$ can be scaled by $K_{IC}$ as:

$$K_{IH} = K_{IC} \exp\left(\frac{-\eta k_{IG}^2 \theta_H}{\alpha'' \sigma_{ys}}\right) \tag{8}$$

In addition, taking the logarithms of Equations (1) and (7) leads to $\ln(\beta' K_{IH}) = (1 - \eta\theta_H)\ln(\beta' K_{IC})$, therefore

$$K_{IH} = \frac{1}{\beta'}(\beta' K_{IC})^{(1-\eta\theta_H)} \tag{9}$$

Equation (9) is the proposed model in this paper, which is very simple and describes the $K_{IH}$ as a function of $K_{IC}$, $\eta$ and $\theta_H$. Based on the Langmuir–McLean isotherm for surface adsorption [36], hydrogen occupancy of interface ($\theta_H$) can be related to the concentration in lattice sites [26,28,37,38] (note that, $\frac{\Gamma}{\Gamma_{max}-\Gamma} = \frac{\theta_H}{1-\theta_H} = C_H \exp\left(\frac{E_b}{RT}\right)$), as:

$$\theta_H = \frac{C_0 \exp\left(\frac{\sigma_H V_H}{RT}\right) \exp\left(\frac{E_b}{RT}\right)}{1 + C_0 \exp\left(\frac{\sigma_H V_H}{RT}\right) \exp\left(\frac{E_b}{RT}\right)} \tag{10}$$

where $E_b$ is hydrogen binding energy with the interface, $R = 8.314\ \mathrm{J/(mol{\cdot}K)}$ is gas constant, $V_H$ is the polar molar volume of hydrogen, $C_0$ is the initial lattice hydrogen concentration (or the hydrogen solubility in equilibrium with the environment in atom fraction in absence of stress), and $\sigma_H$ is the hydrostatic stress at crack tip. Equation (10) considers the enhancement of stress and hydrogen trapping on local hydrogen concentration. For a given material, $\beta'$ and $K_{IC}$ are constants, $\eta$ and $\theta_H$ have their physical origins and can be calculated by Equations (6) and (10), respectively. Therefore, the model can be used to predict the hydrogen-influenced CSIF directly.

## 3. Model Validation

In order to validate the model in predicting $K_{IH}$, parameters including $\Delta g_{int}^0$, $\Delta g_{FS}^0$, $\Gamma_{max}$ and $E_b$, etc., needed to be determined beforehand. Although all these parameters are physically based, not all of them can be collected precisely for a given material at present due to inadequate experimental work. Table 1 shows the parameters recommended for Inconel 690 alloy by Liang et al. [27] and high strength martensitic steels [28,30] when the TDD theory was implemented in their HAF numerical simulations. These values were obtained by either experimental measurements or theorical calculations [27,28,30]. Using Equation (6), the corresponding parameters can be calculated, i.e., $\eta = 0.47$ and 1.36, respectively, for Inconel 690 alloy and martensitic steels. The calculated $\eta$ of Inconel 690 alloy was very close to the one obtained by first-principle calculations for Ni-$\sum$5(012) grain boundary as shown in Figure 1. However, the martensitic steels had a higher $\eta$ (>1), due to a relatively higher $\Gamma_{max}$ ($8.08 \times 10^{-5}$ mol/m$^2$) [30].

**Table 1.** Thermodynamic decohesion parameters recommended in the literature for Inconel 690 alloy [27] and high-strength martensitic steel [28,30].

| Parameter | Alloy 690 | Martensitic Steel |
|---|---|---|
| $\gamma_{FS}/J{\cdot}m^{-2}$ | 2.28 | 1.95 |
| $\gamma_{int}/J{\cdot}m^{-2}$ | 0.866 | 0.78 |
| $2\gamma^0_{int} = (2\gamma_{FS} - \gamma_{int})/J{\cdot}m^{-2}$ | 3.694 | 3.12 |
| $\Delta h^0_{int}/kJ{\cdot}mol^{-1}$ | −26 | −47.4 |
| $\Delta s^0_{int}/J{\cdot}mol^{-1}{\cdot}K^{-1}$ | 25 | 25 |
| $\Delta g^0_{int} = (\Delta h^0_{int} - T\Delta s^0_{int})/kJ{\cdot}mol^{-1}$ | −33.45 | −54.85 |
| $\Delta h^0_{FS}/kJ{\cdot}mol^{-1}$ | −96.37 | −95.5 |
| $\Delta s^0_{FS}/J{\cdot}mol^{-1}{\cdot}K^{-1}$ | 15 | 15 |
| $\Delta g^0_{FS} = (\Delta h^0_{FS} - T\Delta s^0_{FS})/kJ{\cdot}mol^{-1}$ | −100.84 | −99.97 |
| $\Gamma_{max}/mol{\cdot}m^{-2}$ | $2.59 \times 10^{-5}$ | $8.08 \times 10^{-5}$ |
| $E_b/kJ{\cdot}mol^{-1}$ | 12 | / |
| $\eta$ | 0.47 | 1.36 |

Note: $\gamma_{FS}$—surface energy, $\gamma_{int}$—interface energy, $2\gamma^0_{int}$—cohesive energy, $\Delta h^0_{int}$—enthalpies of hydrogen segregation to an interface, $\Delta s^0_{int}$—entropies of hydrogen segregation to an interface, $\Delta g^0_{int}$—Gibbs free energy excess of hydrogen segregation to an interface, $\Delta h^0_{FS}$—enthalpies of hydrogen absorption at a free surface, $\Delta s^0_{FS}$ entropies of hydrogen absorption at a free surface, $T$—temperature, $\Gamma_{max}$—saturated hydrogen coverage, $E_b$—hydrogen trap binding energy, $\eta$—calculated by Equation (6).

Hydrostatic stress ahead of a mode I crack tip can be given by $\sigma_H = n\sigma_{ys}$. For a blunt crack tip, the classical continuum fracture mechanics theory ($J_2$) predicts $n = 3 \sim 5$, depending on the corresponding work-hardening behavior. For an atomistically-sharp intergranular crack tip, $n$ is calculated between 4 to 7 in a dislocation-free zone ahead of crack tip [39]. Gerberich et al. [40] suggested a higher $n$ (8~13) through the computational simulations based on discretized dislocation model. In this work, we took $n = 4$, since a higher $\Gamma_{max}$ had already been used. On the other hand, it was proved that $n \approx 4$ predicted well in finite element simulations [41] and other models [12,16,42] compared with experimental data. Moreover, according to HELP theory, hydrogen can reduce the initial yield stress [14,15], which is equivalent to the drop of $n$.

Experimentally measured CSIF of Inconel 690, 625 and 718 alloy as a function of different initial hydrogen concentrations have been reported [43,44]. Using the parameters recommended by Liang et al. [27] for Inconel 690 alloy and crack tip hydrostatic stress $\sigma_H = 4\sigma_{ys}$, the CSIF values of these three nickel-based alloys were also predicted directly by Equation (9). Figure 2 shows the comparison between the predicted CSIF and the measured results reproduced from Refs. [43,44]. It is obvious that the predicted values using Equation (9) are consistent with the experimental results of the three nickel-based alloys, validating the applicability of the model.

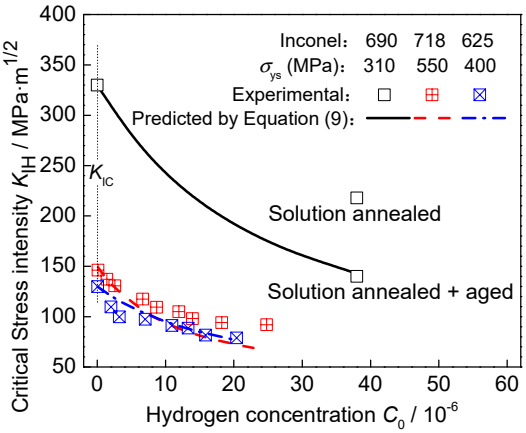



**Figure 2.** Comparisons between predicted values by Equation (9) and experimental values of critical stress intensity factor (CSIF) for three nickel-based alloys reproduced from [43,44] (Inconel 690, 718 and 625) as a function of initial hydrogen concentration (the values of Inconel 690 alloy in the figure were obtained by $K = \left[JE/\left(1-\nu^2\right)\right]^{1/2}$, $J$ is the J-integral given in the reference [43], "solution annealed" means the materials were solution annealed at 1100 °C for 4 h followed by air cooling, and "aged" means aged at 718 °C for 10 h). In order to keep consistent with the references, $C_0$ is in weight ratio in the figure, which should be transformed to atomic ratio when using Equation (9).

As aforementioned, many previous models introduced the empirical coefficient which cannot be determined in advance, therefore a fitting method was often used. Clearly, fitting is unnecessary for the model of Equation (9) as each parameter in the model corresponds to a specific physical variable which can be determined in advance by experimental measurements or theorical calculations. However, in order to avoid the complex processing of all parameters for a given metal, Equation (9) was also validated by fitting a series of experimental data [19,21,45–49] reported for different materials by selecting $E_b$ and $\eta$ as the fitting parameters. The other parameters are set as constants using the values reported in the literature [1,2,18–21,27,50], as listed in Table 2. Figure 3 shows the fitting curves and obtained $E_b$ and $\eta$ values. It is shown that all experimental data can be fitted very well by Equation (9), which further verifies that Equation (9) is applicable and accurate even though some parameters are assigned as constant to reduce the number of variables to be fitted. It was also found that the $\eta$ and $E_b$ values obtained by fittings were in the common range of these two parameters ($\eta$ ranges from 0.2 to 1 and $E_b$ ranges from 10 to 25 kJ/mol for these materials). Moreover, Figure 3e,f indicate that $\eta$ increased with decreasing temperature, in line with the experimental observation that decreasing temperature enhances HAC [48,49].

**Table 2.** Values for parameters [1,2,18–21,27,50] used in the fittings of experimental data by Equation (9).

| Parameter | Value | Parameter | Value |
|---|---|---|---|
| $\alpha''$ /MPa·m | $2 \times 10^{-4}$ | $\beta'$ /MPa$^{-1}$·m$^{-1/2}$ | 0.26 |
| $E$/GPa | 200 | $v$ | 0.3 |
| $V_H$/m$^3$·mol$^{-1}$ | $2 \times 10^{-6}$ | $\Gamma_{max}$/mol·m$^{-2}$ | $2.7 \times 10^{-5}$ |

Note: $\alpha''$, $\beta'$—stress field constants determined by computer simulation, $E$—Young's modulus, $v$—Poisson ratio, $V_H$—polar molar volume of hydrogen, $\Gamma_{max}$—saturated hydrogen coverage.

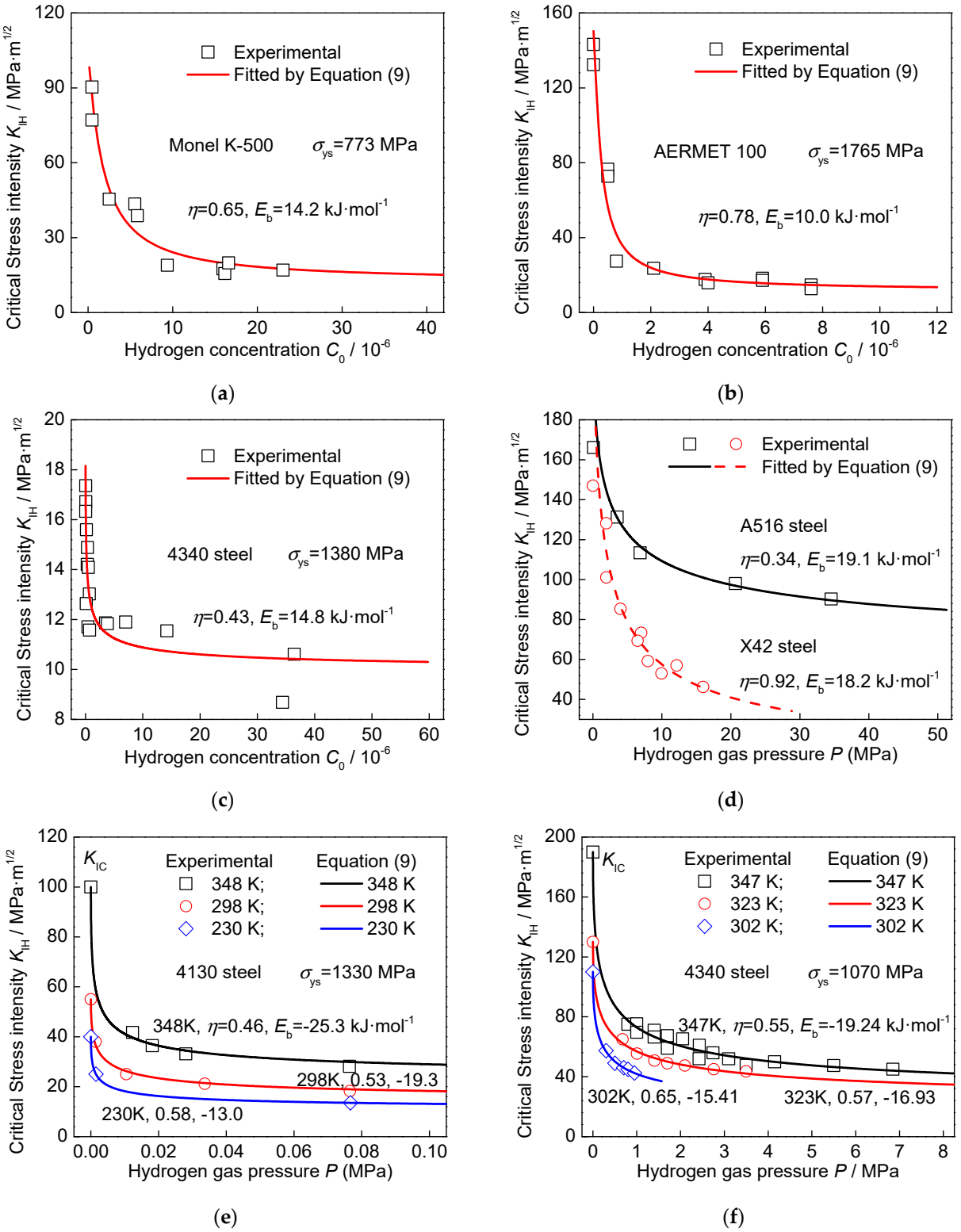



**Figure 3.** Comparisons between experimental data in the literature and fitting curves based on Equation (9) for critical stress intensity factor (CSIF) of metals. (**a**) Monel K-500 high strength Ni-based alloy [21]; (**b**) AERMET 100 ultrahigh-strength steel [19]; (**c**) AISI 4340 high strength steel [45]; (**d**) A516 carbon steel [46] and X42 pipeline steel [47]; (**e**) AISI 4130 high strength steel [48] with temperature effect; (**f**) AISI 4340 high strength steel [49] with temperature effect. In (**a**–**c**), $C_0$ is in weight ratio, which should be transformed to atomic ratio when using Equation (9). In (**d**–**f**), $C_0 = S_0\sqrt{P}$, where $S_0 = 180\frac{\text{mol } H_2}{m^3\Delta\sqrt{\text{MPa}}}\exp\left(\frac{-23.66\text{ KJ/mol}}{RT}\right)$ [12] is the Sieverts solubility constant, $P$ is hydrogen gas pressure.

It has been suggested that, for precipitation-hardened alloys containing cleavage planes or grain boundaries decorated by precipitates, the precipitates are responsible for the decohesion of the interfaces, as they constitute the sites of decohesion due to increase of interfacial stress caused by impingements of dislocation pile-ups onto the precipitates and the reduction of interface cohesive strength caused by the presence of hydrogen [27–30]. Liang and Sofronis [27] have reported that carbide-matrix interface decohesion can produce microcracks propagating along a grain boundary. Ai et al. [51] identified an $E_b$ value of $10.2 \pm 4.6$ kJ/mol for the $Ni_3Al$ precipitates, which are major reversible trap sites decorated along various interfaces in aged Monel K-500 alloy, while Li et al. [52] obtained the value of 11.5 kJ/mol for the $M_2C$ precipitates in AERMET 100 steel. Clearly, these two experimental $E_b$ values are very close to the ones obtained by the fittings, i.e., 14.2 kJ/mol for Monel K-500 alloy (Figure 3a) and 10.0 kJ/mol for AERMET 100 steel (Figure 3b). This indicates that these $E_b$ values obtained by fittings in Figure 3 are credible.

## 4. Discussion

Assuming that microscopic fracture parameters such as local fracture stress/energy decreased linearly as local hydrogen concentration increased, Oriani and Josephic [7], Akhurst and Baker [8], Lee and Unger [9], Unger [10] and Wang et al. [12] proposed their models to evaluate the macroscopic fracture properties such as the crack growth CSIF. However, the linearly decreasing coefficients they introduced cannot be known in advance due to the lack of physical origins. In this paper, we proposed a physically based simple model by combining the MSCG model and TDD theory. The model can provide a direct prediction for the macroscale CSIF of materials with hydrogen influence, as all parameters in the model have clear physical origins and are measurable or calculable.

In Equation (9), $\eta$ is a unitless parameter and $C_0$ is in atom ratio. Analyzing Equation (10), it can be further found that when the initial hydrogen concentration $C_0$ is small, Equation (10) can be simplified as $\theta_H = C_0 \exp(\sigma_h V_H / RT) \exp(E_b / RT)$, at this point, $\theta_H$ is proportional to $C_0$. However, when $C_0$ increases, $\theta_H$ approaches gradually to 1.

In Gerberich's model, Equation (2), the unit of coefficient $\alpha$ depends on the unit of $C_H$. There is no limit on the selection of the unit of $C_H$. Taking account of the hydrostatic stress effect and hydrogen trapping effect on hydrogen concentration, $C_H = C_0 \exp(\sigma_h V_H / RT) \exp(E_b / RT)$. However, if we divide Equation (2) by Equation (1), we can obtain the following relationship, as:

$$\frac{K_{IH}}{K_{IC}} = \exp\left[\frac{(k_{IG} - \alpha C_H)^2 - k_{IG}^2}{\alpha'' \sigma_{ys}}\right] = \exp\left[\frac{(\alpha C_H)^2 - 2\alpha k_{IG} C_H}{\alpha'' \sigma_{ys}}\right] \tag{11}$$

If the hydrogen concentration is low, i.e., $C_H < 1$, we have $(\alpha C_H)^2 \ll 2\alpha k_{IG} C_H$. In fact, it has been reported that a few ppm of hydrogen concentration is enough to induce HAF for high-strength steels, particularly for ultrahigh-strength steels. Thus, ignoring $(\alpha \theta_H)^2$, Equation (11) can be approximated as:

$$\frac{K_{IH}}{K_{IC}} = \exp\left[\frac{-2\alpha k_{IG} C_H}{\alpha'' \sigma_{ys}}\right] \tag{12}$$

Clearly, if the hydrogen concentration $C_H$ in Equation (12) also uses the unit of atom ratio, $C_H$ is approximately equal to $\theta_H$ in amount at the low level of hydrogen concentration. At this point, replacing the local hydrogen concentration term $C_H$ with $\theta_H$, Equation (12) shows the same form with Equation (8) and

$$\alpha = \frac{\eta}{2} k_{IG} \tag{13}$$

It is indicated that model Equations (2) and (8) are equivalent to the condition of low hydrogen concentration level and the empirical parameter $\alpha$ postulated by Gerberich et al. [1,2] can be replaced by $\eta k_{IG}/2$. $\alpha$ has no clear physical origin, but $\eta$ and $k_{IG}$ are

physically based, which can be measured or calculated. In fact, Equation (8) can be approximated by its first order of Taylor series expansion, given as:

$$\frac{K_{IH}}{K_{IC}} \approx 1 - \lambda\theta_H \tag{14}$$

where $\lambda = \frac{-\eta k_{IG}^2}{\alpha'' \sigma_{ys}}$ is a constant for a given material. As known, $\sigma_H/\sigma_C = K_{IH}/K_{IC}$, where $\sigma_H$ and $\sigma_C$ are the local fracture stress with and without hydrogen influence, respectively. The analysis explains why the models based on the assumption that fracture stress is linearly degraded by concentration of hydrogen can lead to good fitting of experimental data. In other words, the TDD theory can provide a physical basis for this assumption and the model is derived from it.

However, if the hydrogen concentration level is gradually increased, $\theta_H$ will approach to 1. Therefore, there is a limit value for hydrogen-influenced $K_{IH}$:

$$\lim_{C_0 \to \infty} K_{IH} = K_{IHmin} = \frac{1}{\beta'}\left(\beta' K_{IC}\right)^{(1-\eta)} \tag{15}$$

This is consistent with experimental trends shown in Figure 3a–c,e,f. It is shown that when hydrogen concentration or hydrogen pressure is increased to a high level, $K_{IH}$ is no longer decreased and remains at a minimal value, $K_{IHmin}$. In fact, this seems to be a common phenomenon. For example, Barthelemy [53] presented the effect of hydrogen partial pressure on rupture pressure in disk rupture tests where hydrogen pressure was increased to a specific level and the helium gas was added until the rupture of the disk. It is shown that the embrittlement index defined as the ratio of helium pressure to hydrogen pressure ($P_{He}/P_{H2}$) increased quickly at low hydrogen partial pressure (before reaching a constant level near 25 bar). However, further increase of hydrogen pressure until 200 bar had no effect on the embrittlement index. Elices and Gutierrez-Solana [47] performed tensile tests on double-notched X42 specimens and showed a ~40% reduction in area loss at hydrogen pressure near 7 MPa. However, increasing the hydrogen pressure to 35 MPa only resulted in a ~50% reduction in area loss. Although the reduction in area loss appears to show a continual increase, it is possible to obtain a critical pressure. Gerberich's model, Equation (2), also shows that $K_{IH}$ decreases with increasing hydrogen concentration; however it will reach to its limit when $k_{IG} \ll \alpha c_H$ and the limit is 0. This clearly make no sense in physics. Therefore, the model, Equation (9), proposed in this paper is more consistent with the experimental data.

It should be noted that, according to Equation (15), the $K_{IHmin}$ values are 15, 10, 11, 60 and 8 MPa$\cdot\sqrt{\text{m}}$, respectively, for Monel K-500 alloy, AERMET 100 ultrahigh-strength steel, AISI 4340 high-strength steel, A516 carbon steel and X42 pipeline steel. Different materials have different $K_{IHmin}$ values. The $K_{IHmin}$ value can be used as a criterion to quantitate and classify the HAF susceptibility of a material. A material with a higher $K_{IHmin}$ is preferred for hydrogen service. Moreover, for a conservative design or safe assessment of a component exposed to a hydrogen-containing environment. It can be believed no matter how much hydrogen is introduced into the component, HAF will not occur when $K_I < K_{IHmin}$.

In addition, as aforementioned, the model does not consider the role of plastic work for simplicity. In fact, plastic work can be involved by using the expression proposed by Jokl et al. [54], which describes the plastic work $\gamma_P$ as a function of $2\gamma_{int}^0$ by $\gamma_P = A\left(2\gamma_{int}^0\right)^q$, where $A$ and $q$ are constants to be determined. At this point, as plastic work is much larger than the reversible work of decohesion, that is, the latter can be ignored ($\gamma_{eff} = 2\gamma_{int}^0 + \gamma_P \approx \gamma_P$), the $k_{IGH}$ can be expressed as $k_{IGH} = k_{IG}\sqrt{(1-\eta\theta_H)^q}$ and thus the model Equation (9) becomes

$$K_{IH} = \frac{1}{\beta'}\left(\beta' K_{IC}\right)^{(1-\eta\theta_H)^q} \tag{16}$$

Using Equation (16) to fit the experimental data of Monel K-500 alloy with different $q$ values, one can see that the data can also be fitted very well with almost no gap between fitting curves ($q = 1$, 2, 4 and 6). With the increase of $q$, the obtained $\eta$ and $E_b$ decreases but $E_b$ tends to plateau after $q > 6$, as shown in Figure 4. Therefore, whether plastic work is considered will not affect the applicability of the model. However, to understand the role of plastic work and quantify its contribution (for example, determining the value of $q$ for different materials), more experimental and theoretical work is needed.

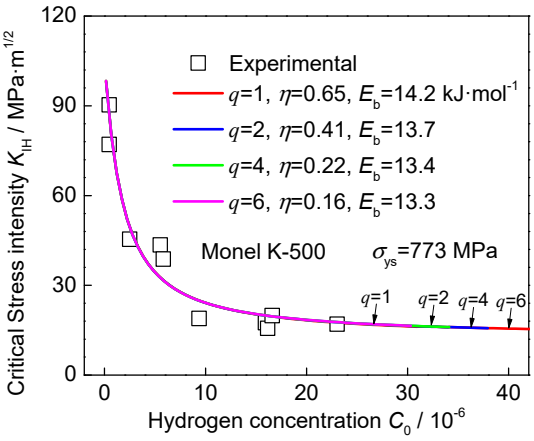



**Figure 4.** The fitting curves based on Equation (10) for critical stress intensity factor (CSIF) of Monel K-500 alloy using different $q$ values.

## 5. Conclusions

This paper proposed a simple physically based model to predict the crack growth critical stress intensity factor (CSIF) with hydrogen influence by combining the microscopically shielded Griffith criterion (MSGC) model and thermodynamics decohesion (TDD) theory. The model predicts the hydrogen-influenced CSIF as a function of the CSIF without hydrogen influence, initial hydrogen concentration or hydrogen solubility, hydrogen trap binding energy and crack tip stress level. The prediction from the model shows good agreement with experimental data reported in the literature. The advantage of the model is that all parameters in the model have physical origins and can be measured or calculated in advance. It can promote the application of stress intensity factor-based crack growth criteria in the design and safety assessment of a metallic component exposing to hydrogen.

**Author Contributions:** Conceptualization, W.W. and Y.W.; methodology, Y.H., W.W. and Y.W.; formal analysis, J.C., Y.H. and W.L.; investigation, J.C., Y.H., W.L., W.W. and Y.W.; data curation, J.C., Y.H., W.L. and Y.W.; writing—original draft preparation, J.C. and Y.H.; writing—review and editing, X.L., Y.W. and Xinyu Yang; validation, Y.W. and Xinyu Yang; visualization, X.L., Y.W. and X.Y.; supervision, X.L., W.W. and Y.W.; project administration, Y.W.; funding acquisition, Y.W. All authors have read and agreed to the published version of the manuscript.

**Funding:** This research was funded by the Fundamental Research Funds for the Central Universities of China, grant number 2019QNA28.

**Institutional Review Board Statement:** Not applicable.

**Informed Consent Statement:** Not applicable.

**Data Availability Statement:** Not applicable.

**Conflicts of Interest:** The authors declare no conflict of interest. The funders had no role in the design of the study; in the collection, analyses, or interpretation of data; in the writing of the manuscript, or in the decision to publish the results.

## References


1. Gerberich, W.W.; Marsh, P.G.; Hoehn, J.W. Hydrogen induced cracking mechanism—Are there critical experiments? In Proceedings of the Fifth International Conference on the Effect of Hydrogen on the Behavior of Materials, Moran, WY, USA, 7 September 1975; The Minerals, Metals, and Materials Society: Warrendale, PA, USA, 1996; p. 539.
2. Gerberich, W.W. Modeling hydrogen induced damage mechanisms in metals. In *Gaseous Hydrogen Embrittlement of Materials in Energy Technologies*; Gangloff, R.P., Somerday, B.P., Eds.; Woodhead Publishing Limited: Cambridge, UK, 2012; Volume 2, p. 209.
3. Gerberich, W.W.; Stauffer, D.D.; Sofronis, P. A coexistent view of hydrogen effects on mechanical behavior of crystals: HELP and HEDE. In Proceedings of the 2008 International Hydrogen Conference—Effects of Hydrogen on Materials, Jackson, WY, USA, 7–10 September 2008; ASM International: Novelty, OH, USA, 2009; p. 38.
4. Gangloff, R.P. Science-based prognosis to manage structural alloy performance in hydrogen. In Proceedings of the 2008 International Hydrogen Conference—Effects of Hydrogen on Materials, Jackson, WY, USA, 7–10 September 2008; ASM International: Novelty, OH, USA, 2009; p. 1.
5. Gerberich, W.W.; Chen, Y.T.; John, C.S. A short-time diffusion correlation for hydrogen-induced crack growth kinetics. *Metall. Trans. A* **1975**, *6*, 1485–1498. [CrossRef]
6. Oriani, R.A. A mechanistic theory of hydrogen embrittlement of steels. *Ber. Bunsenges. Für. Phys. Chem.* **1972**, *76*, 848–857.
7. Oriani, R.; Josephic, P. Equilibrium and kinetic studies of the hydrogen-assisted cracking of steel. *Acta Metall.* **1977**, *25*, 979–988. [CrossRef]
8. Akhurst, K.N.; Baker, T.J. The threshold stress intensity for hydrogen-induced crack growth. *Metall. Mater. Trans. A* **1981**, *12*, 1059–1070. [CrossRef]
9. Lee, S.L.; Unger, D.J. A decohesion model of hydrogen assisted cracking. *Eng. Fract. Mech.* **1988**, *31*, 647–660. [CrossRef]
10. Unger, D.J. A mathematical analysis for impending hydrogen assisted crack propagation. *Eng. Fract. Mech.* **1989**, *34*, 657–667. [CrossRef]
11. Song, J.; Curtin, W.A. Atomic mechanism and prediction of hydrogen embrittlement in iron. *Nat. Mater.* **2013**, *12*, 145–151. [CrossRef]
12. Wang, Y.; Gong, J.; Jiang, W. A quantitative description on fracture toughness of steels in hydrogen gas. *Int. J. Hydrogen Energy* **2013**, *38*, 12503–12508. [CrossRef]
13. Huang, S.; Zhang, Y.; Yang, C.; Hu, H. Fracture strain model for hydrogen embrittlement based on hydrogen enhanced localized plasticity mechanism. *Int. J. Hydrogen Energy* **2020**, *46*, 25541–25554. [CrossRef]
14. Sofronis, P.; Liang, Y.; Aravas, N. Hydrogen induced shear localization of the plastic flow in metals and alloys. *Eur. J. Mech. Solids* **2001**, *20*, 857–872. [CrossRef]
15. Djukic, M.B.; Bakic, G.M.; Zeravcic, V.S.; Sedmak, A.; Rajicic, B. The synergistic action and interplay of hydrogen embrittlement mechanisms in steels and iron: Localized plasticity and decohesion. *Eng. Fract. Mech.* **2019**, *216*, 106528. [CrossRef]
16. Traidia, A.; Chatzidouros, E.; Jouiad, M. Review of hydrogen-assisted cracking models for application to service lifetime prediction and challenges in the oil and gas industry. *Corros. Rev.* **2018**, *36*, 323–347. [CrossRef]
17. Geng, W.T.; Wang, V.; Li, J.-X.; Ishikawa, N.; Kimizuka, H.; Tsuzaki, K.; Ogata, S. Hydrogen trapping in carbon supersaturated $\alpha$-iron and its decohesion effect in martensitic steel. *Scr. Mater.* **2018**, *149*, 79–83. [CrossRef]
18. Martínez-Pañeda, E.; Niordson, C.F.; Gangloff, R.P. Strain gradient plasticity-based modeling of hydrogen environment assisted cracking. *Acta Mater.* **2016**, *117*, 321–332. [CrossRef]
19. Thomas, R.L.S.; Scully, J.R.; Gangloff, R.P. Internal hydrogen embrittlement of ultrahigh-strength AERMET 100 steel. *Metall. Mater. Trans. A* **2003**, *34*, 327–344. [CrossRef]
20. Lee, Y.; Gangloff, R.P. Measurement and Modeling of Hydrogen Environment–Assisted Cracking of Ultra-High-Strength Steel. *Metall. Mater. Trans. A* **2007**, *38*, 2174–2190. [CrossRef]
21. Gangloff, R.P.; Ha, H.M.; Burns, J.T.; Scully, J.R. Measurement and Modeling of Hydrogen Environment-Assisted Cracking in Monel K-500. *Metall. Mater. Trans. A* **2014**, *45*, 3814–3834. [CrossRef]
22. Burns, J.T.; Harris, Z.; Dolph, J.D.; Gangloff, R.P. Measurement and Modeling of Hydrogen Environment-Assisted Cracking in a Ni-Cu-Al-Ti Superalloy. *Metall. Mater. Trans. A* **2016**, *47*, 990–997. [CrossRef]
23. Zhang, T.; Chu, W.; Gao, K.; Qiao, L. Study of correlation between hydrogen-induced stress and hydrogen embrittlement. *Mater. Sci. Eng. A* **2003**, *347*, 291–299. [CrossRef]
24. Wang, R. Effects of hydrogen on the fracture toughness of a X70 pipeline steel. *Corros. Sci.* **2009**, *51*, 2803–2810. [CrossRef]
25. Hirth, J.P.; Rice, J.R. On the thermodynamics of adsorption at interfaces as it influences decohesion. *Metall. Trans. A* **1980**, *11*, 1501–1511. [CrossRef]
26. Wang, J.-S. The thermodynamics aspects of hydrogen induced embrittlement. *Eng. Fract. Mech.* **2001**, *68*, 647–669. [CrossRef]
27. Liang, Y.; Sofronis, P. Toward a phenomenological description of hydrogen-induced decohesion at particle/matrix interfaces. *J. Mech. Phys. Solids* **2003**, *51*, 1509–1531. [CrossRef]
28. Novak, P.; Yuan, R.; Somerday, B.; Sofronis, P.; Ritchie, R. A statistical, physical-based, micro-mechanical model of hydrogen-induced intergranular fracture in steel. *J. Mech. Phys. Solids* **2010**, *58*, 206–226. [CrossRef]
29. Jung, S.-P.; Kwon, Y.; Lee, C.S.; Lee, B.-J. Influence of hydrogen on the grain boundary crack propagation in bcc iron: A molecular dynamics simulation. *Comp. Mater. Sci.* **2018**, *149*, 424–434. [CrossRef]

30. Nagao, A.; Dadfarnia, M.; Somerday, B.P.; Sofronis, P.; Ritchie, R.O. Hydrogen-enhanced-plasticity mediated decohesion for hydrogen-induced intergranular and "quasi-cleavage" fracture of lath martensitic steels. *J. Mech. Phys. Solids* **2018**, *112*, 403–430. [CrossRef]
31. Huang, H.; Gerberich, W. Quasi-equilibrium modeling of the toughness transition during semibrittle cleavage. *Acta Metall. Mater.* **1994**, *42*, 639–647. [CrossRef]
32. Marsh, P.; Gerberich, W. A microscopically-shielded Griffith criterion for cleavage in grain oriented silicon steel. *Acta Metall. Mater.* **1994**, *42*, 613–619. [CrossRef]
33. Zielinski, W.; Lii, M.J.; Gerberich, W.W. Crack-tip dislocation emission arrangements for equilibrium—I. In situ TEM observations of Fe–2wt%Si. *Acta Metall. Mater.* **1992**, *40*, 2861–2871. [CrossRef]
34. Jiang, D.; Carter, E.A. First principles assessment of ideal fracture energies of materials with mobile impurities: Implications for hydrogen embrittlement of metals. *Acta Mater.* **2004**, *52*, 4801–4807. [CrossRef]
35. Jensen, I.J.T.; Olden, V.; Løvvik, O.M. Decohesion energy of ∑5(012) grain boundaries in Ni as function of hydrogen content. *Metall. Mater. Trans. A* **2019**, *50*, 451–456. [CrossRef]
36. Hondros, E.D.; Seah, M.P. The theory of grain boundary segregation in terms of surface adsorption analogues. *Metall. Trans. A* **1977**, *8*, 1363–1371. [CrossRef]
37. Serebrinsky, S.; Carter, E.A.; Ortiz, M. A quantum-mechanically informed continuum model of hydrogen embrittlement. *J. Mech. Phys. Solids* **2004**, *52*, 2403–2430. [CrossRef]
38. Song, J.; Curtin, W. A nanoscale mechanism of hydrogen embrittlement in metals. *Acta Mater.* **2011**, *59*, 1557–1569. [CrossRef]
39. Kameda, J. A microscopic model of hydrogen-induced intergranular cracking—I. Equilibrium crack growth. *Acta Metall.* **1986**, *34*, 867–882. [CrossRef]
40. Gerberich, W.W.; Oriani, R.A.; Lji, M.-J.; Chen, X.; Foecke, T. The necessity of both plasticity and brittleness in the fracture thresholds of iron. *Philos. Mag. A* **1991**, *63*, 363–376. [CrossRef]
41. Olden, V.; Thaulow, C.; Johnsen, R.; Østby, E.; Berstad, T. Application of hydrogen influenced cohesive laws in the prediction of hydrogen induced stress cracking in 25%Cr duplex stainless steel. *Eng. Fract. Mech.* **2008**, *75*, 2333–2351. [CrossRef]
42. Cheng, A.; Chen, N.-Z. Fatigue crack growth modelling for pipeline carbon steels under gaseous hydrogen conditions. *Int. J. Fatigue* **2017**, *96*, 152–161. [CrossRef]
43. Symons, D.M. The effect of carbide precipitation on the hydrogen-enhanced fracture behavior of alloy 690. *Metall. Mater. Trans. A* **1998**, *29*, 1265–1277. [CrossRef]
44. Hicks, P.D.; Altstetter, C.J. Hydrogen-enhanced cracking of superalloys. *Met. Mater. Trans. A* **1992**, *23*, 237–249. [CrossRef]
45. Walter, R.J.; Chandler, W.T. *Influence of Gaseous Hydrogen on Metals*; A Report (NASA-CR-124410) of Marshall Space Flight Center of NASA; NASA: Huntsville, AL, USA, 1973.
46. Robinson, S.L.; Stoltz, R.E. Toughness losses and fracture behavior of low strength carbon-manganese steels in hydrogen. In Proceedings of the Third International Conference on Effect of Hydrogen on Behavior of Materials; The Metallurgical Society of AIME: Warrendale, PA, USA, 1981; p. 987.
47. Gutierrez-Solana, F.; Elices, M. High-pressure hydrogen behavior of a pipeline steel. In Proceedings of the First International Conference on Current Solutions to Hydrogen Problems in Steels; ASM International: Novelty, OH, USA, 1982; p. 181.
48. Nelson, H.G.; Williams, D.P. *Quantitative Observations of Hydrogen-Induced, Slow Crack Growth in a Low Alloy Steel*; A Report of Ames Research Center of NASA; NASA: Santa Clara, CA, USA, 1977.
49. Story, G.C. Hydrogen Assisted Cracking of a Low Alloy Steel–Pressure, Temperature and Yield Strength Effects on the Threshold Fracture Toughness. Ph.D. Thesis, University of California-Davis, Davis, CA, USA, 1980.
50. Kirchheim, R.; Somerday, B.; Sofronis, P. Chemomechanical effects on the separation of interfaces occurring during fracture with emphasis on the hydrogen-iron and hydrogen-nickel system. *Acta Mater.* **2015**, *99*, 87–98. [CrossRef]
51. Ai, J.-H.; Ha, H.M.; Gangloff, R.P.; Scully, J.R. Hydrogen diffusion and trapping in a precipitation-hardened nickel–copper–aluminum alloy Monel K-500 (UNS N05500). *Acta Mater.* **2013**, *61*, 3186–3199. [CrossRef]
52. Li, D.; Gangloff, R.P.; Scully, J.R. Hydrogen trap states in ultrahigh-strength AERMET 100 steel. *Metall. Mater. Trans. A* **2004**, *35*, 849–864. [CrossRef]
53. Barthélémy, H. Effects of pressure and purity on the hydrogen embrittlement of steels. *Int. J. Hydrogen Energy* **2011**, *36*, 2750–2758. [CrossRef]
54. Jokl, M.; Vitek, V.; McMahon, C. A microscopic theory of brittle fracture in deformable solids: A relation between ideal work to fracture and plastic work. *Acta Metall.* **1980**, *28*, 1479–1488. [CrossRef]